Hu *et al. eLight* (2022) 2:2
https://doi.org/10.1186/s43593-021-00009-5

Official Journal of CIOMP
elight.springeropen.com

RESEARCH ARTICLE Open Access

Surface Dyakonov–Cherenkov radiation

Hao Hu[1†], Xiao Lin[2,3†], Liang Jie Wong[1], Qianru Yang[1], Dongjue Liu[1], Baile Zhang[4,5*] and Yu Luo[1,6*]

Abstract

Recent advances in engineered material technologies (e.g., photonic crystals, metamaterials, plasmonics, etc.) provide valuable tools to control Cherenkov radiation. In all these approaches, however, the particle velocity is a key parameter to affect Cherenkov radiation in the designed material, while the influence of the particle trajectory is generally negligible. Here, we report on surface Dyakonov–Cherenkov radiation, i.e. the emission of directional Dyakonov surface waves from a swift charged particle moving atop a birefringent crystal. This new type of Cherenkov radiation is highly susceptible to both the particle velocity and trajectory, e.g. we observe a sharp radiation enhancement when the particle trajectory falls in the vicinity of a particular direction. Moreover, close to the Cherenkov threshold, such a radiation enhancement can be orders of magnitude higher than that obtained in traditional Cherenkov detectors. These distinct properties allow us to determine simultaneously the magnitude and direction of particle velocities on a compact platform. The surface Dyakonov–Cherenkov radiation studied in this work not only adds a new degree of freedom for particle identification, but also provides an all-dielectric route to construct compact Cherenkov detectors with enhanced sensitivity.

Keywords: Cherenkov radiation, Dyakonov surface wave, Particle detector

1 Introduction

Cherenkov radiation arises when a charged particle moves with a velocity exceeding the phase velocity of light in a transparent medium [1, 2]. In transparent dielectric materials, Cherenkov radiation is an extended mode (i.e., a packet of Cherenkov photons) propagating into the infinity at a constant emission angle θ_c. This so-called Cherenkov angle depends on the particle velocity v as $\cos\theta_c = \frac{c}{nv}$ [3], where c is the light speed in the vacuum and n is the refractive index of the background medium. As a key application in particle physics, Cherenkov radiation has been widely deployed for particle discrimination, i.e. the particle velocity can be determined with high accuracy by measuring the Cherenkov angle of emitted photons [4–9]. Emerging communication applications call for a route map towards the miniaturization of Cherenkov devices [10–15]. However, the major challenge to scale down Cherenkov detectors arises from the large footprint of photon detection apparatus.

In recent decades, surface waves have drawn extensive attention in nanotechnology owing to their ability to confine electromagnetic waves in subwavelength domains [16–19]. Surface plasmon-polariton (SPP) existing at metal/dielectric interfaces is perhaps the most well-known example [20–23]. Its enhanced photonic density of states leads to a wealth of nanotechnological breakthroughs in super-resolution imaging, ultrasensitive biosensing, efficient light emission, etc [24–26]. On the other hand, light–matter interactions with surface phonon-polariton (SPhP) at the interface of van der Waals materials attracts increased research interest mainly due to the high confinement and moderate losses of SPhP in the mid-infrared frequency [27, 28]. Especially, recent advances in particle physics have shown that SPPs/SPhPs may also provide a route to control Cherenkov radiation at the subwavelength scale [29, 30]. This so-called surface-polariton Cherenkov radiation exhibits several

*Correspondence: blzhang@ntu.edu.sg; luoyu@ntu.edu.sg
†Hao Hu and Xiao Lin contributed equally to this work
[1] School of Electrical and Electronic Engineering, Nanyang Technological University, 50 Nanyang Avenue, Singapore 639798, Singapore
[4] Division of Physics and Applied Physics, School of Physical and Mathematical Sciences, Nanyang Technological University, 21 Nanyang Link, Singapore 637371, Singapore
Full list of author information is available at the end of the article

Springer Open

© The Author(s) 2022. **Open Access** This article is licensed under a Creative Commons Attribution 4.0 International License, which permits use, sharing, adaptation, distribution and reproduction in any medium or format, as long as you give appropriate credit to the original author(s) and the source, provide a link to the Creative Commons licence, and indicate if changes were made. The images or other third party material in this article are included in the article's Creative Commons licence, unless indicated otherwise in a credit line to the material. If material is not included in the article's Creative Commons licence and your intended use is not permitted by statutory regulation or exceeds the permitted use, you will need to obtain permission directly from the copyright holder. To view a copy of this licence, visit http://creativecommons.org/licenses/by/4.0/.

unique features including enhanced photon emission, reversed Cherenkov cone and vanishing Cherenkov threshold [31–38]. However, realization of miniaturized Cherenkov detectors with SPPs/SPhPs is still challenging, probably because of the non-negligible dissipation losses and strong chromatic dispersion of used materials [39]. For instance, the large metallic dissipation inevitably prohibits the detection of surface-polariton Cherenkov radiation beyond the plasmon propagation length (which is usually several micrometers at optical frequencies). On the other hand, the strong chromatic dispersion makes the emission angle of surface-polariton Cherenkov radiation highly wavelength-dependent and therefore unavoidably limits the working bandwidth of designed Cherenkov detectors. These problems become more severe when the particle velocity approaches the Cherenkov threshold, where the photon emission is inherently weak. Hence, an alternative approach with suppressed dissipation and dispersion effects is still highly demanded for the design of compact Cherenkov detectors.

Here, we show that Dyakonov surface waves (DSWs) supported by transparent birefringent materials provide a feasible solution to these problems [40]. We investigate systematically surface Dyakonov–Cherenkov radiation at the surface of a birefringent crystal in contact with an isotropic background medium and find that the emission behaviors are strongly susceptible to the particle velocity and trajectory. Remarkably, the excitation of DSWs significantly enhances the photon emission by several orders of magnitude when the particle velocity approaches to the threshold velocity of the swift charge in surrounding medium. This unique feature greatly facilitates the particle identification around the velocity cutoff. In addition, DSWs have another two distinct advantages over conventional surface plasmons: first, their negligible dissipation losses not only enhance the photon extraction efficiency, but also significantly increase the propagation length of surface waves, facilitating the far-field detection of Cherenkov signals; second, their small chromatic dispersion dramatically broadens the working bandwidth of particle detectors. Our studies add a new perspective on enhanced particle–photon–matter interactions and open up an opportunity for achieving high-performance Cherenkov detectors on chip.

2 Results and discussions

Without loss of generality, we consider a swift charged particle of velocity $\bar{v}$ travelling parallel to the interface of an isotropic background medium (with a refractive index n_a) and a uniaxial birefringent crystal (with ordinary and extraordinary refractive indices denoted as n_o and n_e, respectively). The distance between the particle trajectory and the interface is $y_0 = 200$ nm. The optical axis of birefringent crystal is orientated parallel to the interface, as shown in Fig. 1a. In this configuration, DSWs exist if $n_e > n_a > n_o$ [41–45]. To satisfy this condition, we choose Si_3N_4 as the isotropic background medium and YVO_4 as the birefringent crystal. The refractive indices of studied materials are $n_a = 2.04$, $n_o = 1.99$ and $n_e = 2.22$. In general, DSWs are highly directional and exist only within small angular regions in four quadrants (i.e., θ_d, $\pi - \theta_d$, $\pi + \theta_d$, $2\pi - \theta_d$), where $\theta_d \in [29.43°, 30.15°]$ is the angle between the phase velocity of DSWs and the optical axis of the YVO_4 crystal. In this study, we focus our discussions on the behaviors of DSWs in the first quadrant. Owing to the mirror symmetry, our results also apply to DSWs in other three quadrants.

We begin our analysis by studying the excitation condition of DSWs by the swift charged particle. Denote θ_q as the angle between the optical axis and the particle trajectory (Fig. 1a). We find that the excitation of Dyakonov surface modes requires θ_q fulfilling the following condition (Additional file 1: Section S4):

$$\theta_q = \theta_d \pm \cos^{-1}\left(\frac{\omega}{k_d v}\right), \tag{1}$$

where ω is the angular frequency; k_d is the magnitude of in-plane wavevector of the Dyakonov surface mode. Unlike conventional Cherenkov photons which can be produced by charged particles travelling along any direction (i.e. regardless of θ_q), Dyakonov surface modes can be excited only for some specific θ_q.

The radiation field pattern from the swift charged particle is very susceptible to the magnitude and direction of the particle velocity in our platform. To illustrate this point and reveal the impact of DSWs, we plot in Fig. 1b–d radiation field patterns for three circumstances. When Eq. (1) is rigorously satisfied, the radiation mode is a superposition of the conventional Cherenkov photons and DSWs, as shown in Fig. 1b. In this case, the radiation field can penetrate deeply into the YVO_4 crystal. Such a large penetration length results from the weak longitudinal confinement of DSWs on the interface [17]. In addition, surface Dyakonov–Cherenkov radiation also features an extremely asymmetric field pattern in the transverse plane (Additional file 1: Fig. S5). On the other hand, when the magnitude or direction of the particle velocity changes slightly such that Eq. (1) is no longer satisfied, the swift charged particle emits only conventional Cherenkov photons. As a result, the radiation field decays rapidly in the YVO_4 crystal (Fig. 1c, d) and the field pattern becomes symmetric in the transverse plane (Additional file 1: Fig. S5). These results clearly demonstrate

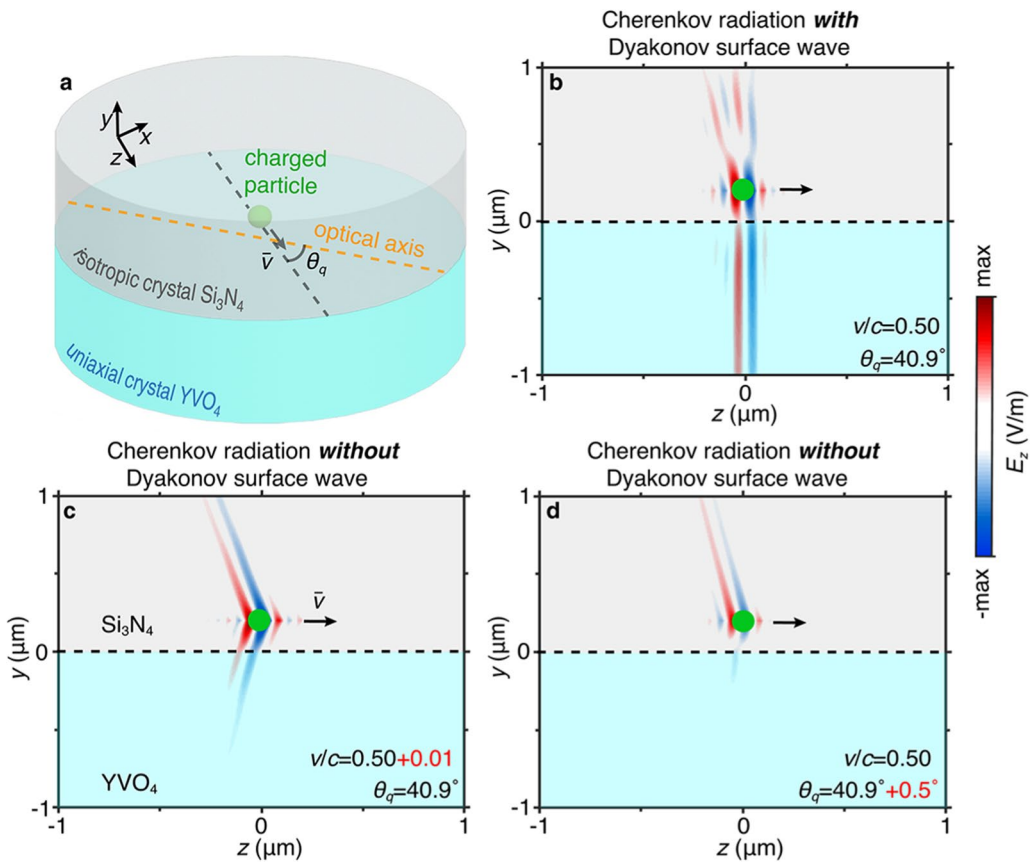

Fig. 1 Emission behaviors of a swift charged particle in an all-dielectric structure made of a semi-infinite istrotropic medium Si_3N_4 and a semi-infinite uniaxial crystal YVO_4. **a** The schematic of the setup. A swift charged particle moves parrallel to the interface between the isotropic medium Si_3N_4 and the uniaxial crystal YVO_4. The angle between the particle velocity and the optical axis of the uniaxial crystal is denoted as θ_q. **b**–**d** Time-domain radiation-field distributions of the charged particle in the cross section formed by the surface normal and the particle trajectory. When $v = 0.50c$ and $\theta_q = 40.9°$, the swift charged particle excites both free-space Cherenkov photons and DSWs in **b**; when v is changed to $0.51c$ (**c**) or θ_q is changed to be 41.4° (**d**), only free-space Cherenkov photons are produced. In all the plots, the distance between the particle trajectory and the interface is fixed as $y_0 = 200$ nm, and the integration range of the wavelength is $\lambda \in [0.2, 2]$ μm in free space

that the excitation of DSWs relies heavily on the particle trajectory. This property provides an effective way to determine simultaneously the particle velocity and trajectory for high-energy particles whose directions are oriented parallel to the surface of the birefringent crystal, through the direct measurement of the radiation field pattern.

Excitation of DSWs modifies not only the near-field pattern, but also the energy loss of the swift particle. As shown in Fig. 2, the power spectral density is quite susceptible to the particle velocity and trajectory, and increases dramatically when Eq. (1) is satisfied. To explore the underlying physical mechanism, we divide the total radiation power into two parts, i.e., the radiation loss G_{ph} through the emission of free-space Cherenkov photons and the radiation loss G_{DSW} through the excitation of DSWs.

Figure 2b, c clarify quantitatively the respective contributions of G_{ph} and G_{DSW} to the total power spectral density at $\lambda = 0.635$ μm. Our results show that G_{ph} and G_{DSW} display distinctly different responses to the particle velocity and trajectory. On the one hand, G_{ph} (as denoted as the straight dashed line) increases smoothly as the particle velocity increases (Fig. 2b) while at the same time remains almost a constant over a broad angular band (Fig. 2c). Such a behavior makes particle detection with traditional Cherenkov photons difficult. On the other hand, G_{DSW} is much more sensitive to small variations in particle velocity/trajectory and acquires a nonzero value only when v and θ_q strictly satisfy the condition given by Eq. (1) (see Fig. 2a and the bulges in Fig. 2b, c). The

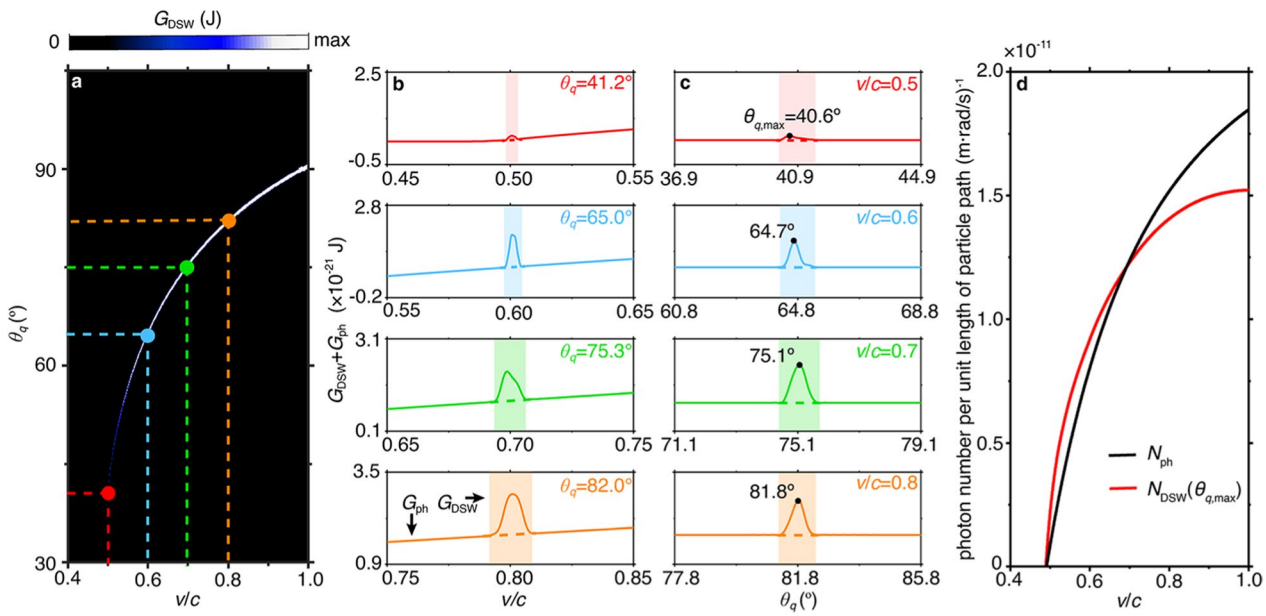

Fig. 2 Energy loss of a swift charged particle emitting Dyakonov surface wave. A power spectral density G_{DSW} (owing to the excitation of DSWs) as a function of the normalized particle velocity v/c and the angle θ_q (corresponding to the orientation of the particle trajectory). G_{DSW} acquires a nonzero value only when v and θ_q satisfy the phase matching condition given by Eq. (1). **b** The total power spectral density $G_{DSW} + G_{ph}$ (where G_{ph} refers to the radiation loss of free-space Cherenkov photons) versus the normalized particle velocity v/c for angle $\theta_q = 40.9°, 64.8°, 75.1°$ and 81.8°, respectively. **c** The total power spectral density $G_{DSW} + G_{ph}$ versus the angle θ_q for particle velocity $v = 0.5c, 0.6c, 0.7c$ and $0.8c$, respectively. $\theta_{q,\max}$ (θ_q at the maximum energy loss) is marked for each velocity in **c**. In particular, we denote G_{ph} as the straight dashed line **b**, **c**. **d** The maximum achievable photon number $N_{DSW}(\theta_{q,\max})$ of DSW generated per unit length of the particle path at each particle velocity. For comparison, we also plot the photon number N_{ph} of free-space Cherenkov radiation as a function of particle velocity. The studied wavelength is 0.635 μm

velocity range for nonzero G_{DSW} is generally smaller than $0.02c$, e.g., from $0.502c$ to $0.498c$, $0.596c$ to $0.604c$, $0.694c$ to $0.706c$, and $0.792c$ to $0.808c$ for $\theta_q = 40.9°, 64.8°, 75.1°$, and 81.8°, respectively; the angular band for nonzero G_{DSW} is generally smaller than 1°, e.g., from 40.4° to 41.4°, 64.3° to 65.3°, 74.6° to 75.6°, and 81.3° to 82.3° for $v = 0.5c$, $0.6c$, $0.7c$, and $0.8c$, respectively. $\theta_{q,\max}$ (i.e., θ_q at the maximum energy loss) shows excellent agreement with θ_q fulfilling Eq. (1). The enhanced sensitivity in energy loss offers an alternative approach to measure simultaneously the particle velocity and trajectory. We also reveal that the maximum achievable photon number $N_{DSW}(\theta_{q,\max})$ of DSW generated per unit length of the particle path is greater than that N_{ph} of free-space Cherenkov radiation in the low-speed regime (i.e., $0.49c < v < 0.7c$), while N_{ph} dominates the total photon number in the high-speed regime (i.e., $0.7c < v < c$) (Fig. 2d). The consideration of realistic chromatic dispersion of materials will not affect our findings (Additional file 1: Figs. S9, S10).

The negligible chromatic dispersion and small dissipation loss of our structure can greatly enhance the photon extraction by means of DSWs, facilitating particle detection in the far field. To highlight this point, we compare the power flow density of surface Dyakonov–Cherenkov radiation with that of surface-polariton Cherenkov radiation [46]. In our comparison, the surface-polariton Cherenkov radiation is investiageted in the plasmonic system made of Aluminum Oxide (Al_2O_3) and Gold (Au), such that the corresponding SPPs have a propagation constant identical to that of DSWs at a wavelength of $\lambda = 0.641$ μm (Additional file 1: Fig. S8). Meanwhile, the distance from the particle trajectory and the interface is set as $y_0 = 0.09\delta$ (with δ as the penetration depth of the surface mode in the superstrate) such that the interaction strengths between the swift charge and surface waves are the same for both configurations. Here, the dielectric constants of Al_2O_3 and Au are taken from the experimental data [47, 48]. Figure 3 demonstrates that DSWs are more strongly excited than conventional SPPs despite of their weak confinement along the longitudinal direction. First, the photon extraction efficiency of DSWs is much higher (i.e. the power flow density is an orders of magnitude larger) than that of conventional SPPs at $l = 0$ μm, as shown in Fig. 3c. Second, DSWs have a much longer propagation distance and remain detectable in the far field, e.g. the Poynting power of DSWs attenuates less than 5% over a distance of 10 μm, while conventional SPPs have already faded away over such a distance. On the other hand, owing to the

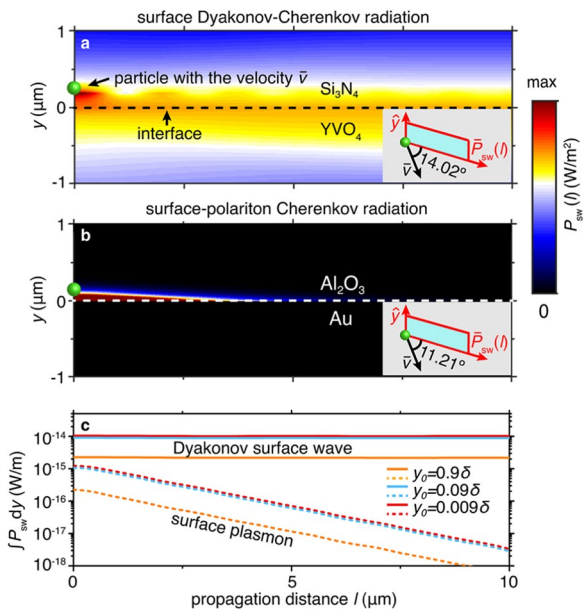

Fig. 3 Comparison between surface Dyakonov–Cherenkov radiation and surface-polariton Cherenkov radiation. **a** The contour plot of the power flow density in the cross section formed by the surface normal $\hat{y}$ and the power flow direction $\overline{P}_{sw}$ of DSWs. **b** The contour plot of the power flow density in the cross section formed by the surface normal $\hat{y}$ and the power flow direction $\overline{P}_{sw}$ of conventional SPPs. In **a**, **b**, $y_0 = 0.09\delta$, which is the penetration depth in the superstrate $\delta = 2.2$ μm ($\delta = 0.1$ μm) for DSWs (SPPs) at $\lambda = 0.641$ μm. The insets of **a**, **b** highlight the orientations of studied cross sections (as marked in cyan) to the particle velocity. **c** The Poynting power $\overline{P}_{sw}$ integrated along the *y*-direction versus the propagation distance *l*, when $y_0 = 0.9\delta$, 0.09δ and 0.009δ, respectively. In our comparison, we choose Si_3N_4–YVO_4 and Al_2O_3–Au as the platforms to excite DSWs and SPPs, respectively, such that the corresponding DSWs and SPPs have an identical effective mode index $n_{eff} = 2.0309$ at $\lambda = 0.641$ μm. The particle velocity is $v = 0.5c$ for both configurations. As a result, DSWs/SPPs propagate in a direction with 14.02°/11.21° to the particle trajectory (see insets of **a**, **b**)

long penetration depth δ_{DSW} (22 times larger than that of SPPs at 0.641 μm), the excitation efficiency of DSWs is robust against the variation of y_0, e.g. from 0 to 200 nm (Fig. 3b). In sharp contrast, the swift particle cannot efficiently excite SPPs when $y_0 > \delta_{SPP} = 100$ nm.

Finally, to demonstrate that surface Dyakonov–Cherenkov radiation can be used for the particle detection, we plot $\theta_{q,\max}$ (i.e. θ_q at the maximum energy loss) as a function of the velocity/momentum of particles. As shown in Fig. 4, measuring $\theta_{q,\max}$ not only determines the particle velocity, but also offers a possible route for the particle discrimination, e.g. $\theta_{q,\max}$ for electron, pion, kaon and proton are 90.45°, 89.55°, 80.41° and 54.35°, respectively, at the momentum of 0.6 GeV/*c*. Such a strong variation in $\theta_{q,\max}$ indicates that our configuration provides a high detection sensitivity when applied to particle detection.

3 Conclusions

We demonstrate that DSWs offer a powerful platform to manipulate Cherenkov radiation at the nanoscale. Different from conventional Cherenkov or surface-polariton Cherenkov radiation, surface Dyakonov–Cherenkov radiation is highly susceptible to the particle trajectory. Small chromatic dispersion and negligible propagation loss make our all-dielectric structure highly suitable for particle detection on chip. We highlight that the birefringence of the host material can strongly impact the behavior of surface Dyakonov–Cherenkov radiation (Additional file 1: Fig. S2). Particularly, larger birefringence gives rise to a larger angular existing domain for DSWs. As a result, surface Dyakonov–Cherenkov radiation becomes less sensitive to the particle trajectory. Thus, the usage of strongly anisotropic materials such as van der Waals materials and hyperbolic metamaterials [47–49] will not lead to our key findings. For the practical implementation, the optical axis orientation (and hence θ_q) can be effectively controlled by constructing a cascade structure and/or applying a Galvo motor [50], providing a route to control surface Dyakonov–Cherenkov radiation (see more discussions in Additional file 1: Section S8).

4 Methods

4.1 Photon emission from a swift charged particle atop the interface between a birefringent crystal and an isotropic background medium

The corresponding setup is depicted in Fig. 1a. In the isotropic dielectric background, the swift charged particle with an effective current density $\overline{J}(\overline{r},t) = \hat{z}vq_0\delta(x)\delta(y-y_0)\delta(z-vt)$ induces a scalar potential, which can be expressed in the frequency domain as

$$\phi_0(\overline{r},\omega) = \int_{-\infty}^{+\infty} \mathrm{d}k_x \frac{\mathrm{i}q_0}{8\pi^2 k_{ya}} \mathrm{e}^{\mathrm{i}k_x x + \mathrm{i}k_{ya}|y-y_0| + \mathrm{i}k_z z}.$$

As a result, the frequency-domain source fields are calculated as,

$$\overline{E}(\overline{r},\omega) = \frac{\mathrm{i}}{\omega\varepsilon_0\varepsilon_a}\nabla\times\nabla\times\left(\hat{z}\phi_0\right),$$

$$\overline{H}(\overline{r},\omega) = \nabla\times\left(\hat{z}\phi_0\right),$$

where $\varepsilon_a = n_a^2$ is the permittivity of the isotropic dielectric. In particular, the source field with the wavevector of $\overline{k}_a^s = \left[\,0\ \ -k_{ya}\ \ k_{in}\,\right]$ in the (u, y, w) coordinate system can be decoupled into *p*- and *s*-polarized field, respectively, where $k_{in} = \sqrt{k_x^2 + k_z^2}$ is the in-plane wavevector. Light incident upon the boundary between the isotropic dielectric and birefringent crystal is reflected as

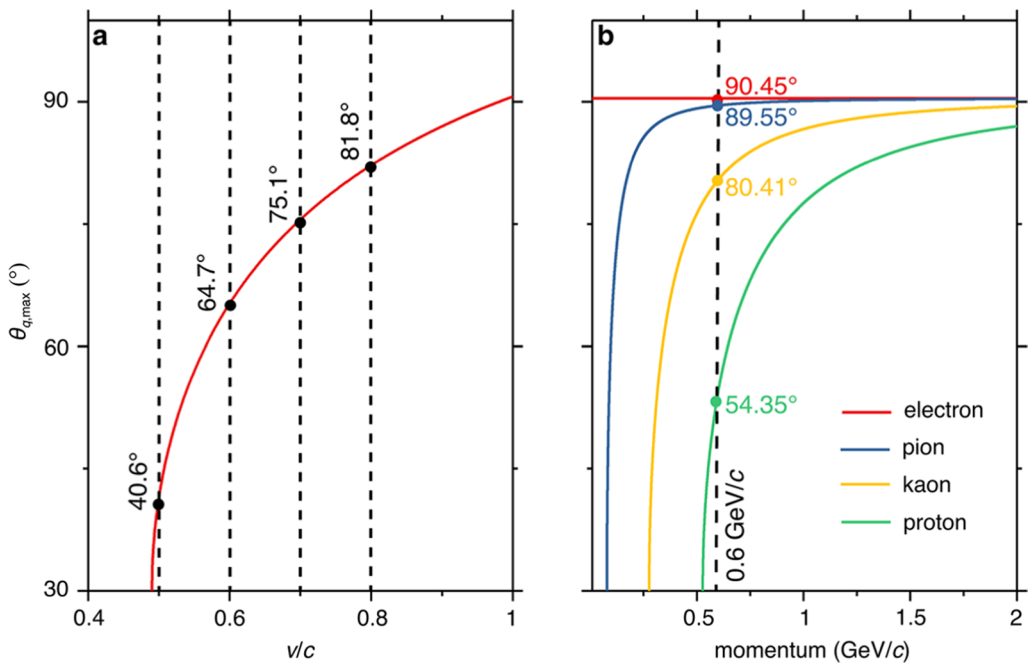

Fig. 4 Particle detection with surface Dyakonov–Cherenkov radiation. a The angle $\theta_{q,\max}$ versus the normalized particle velocity v/c. **b** The angle $\theta_{q,\max}$ versus the particle momenta for four elementary particles

p- and s-polarized light, while transmitted as *ordinary (o)* and *extraordinary (e)* light. Wavevectors of reflected as p- and s-polarized light are identical and given by $\overline{k}_a = \left[\,0\ k_{ya}\ k_{\text{in}}\,\right]$, while wavevectors of transmitted o and e light are different and given by $\overline{k}_o = \left[\,0\ -k_{yo}\ k_{\text{in}}\,\right]$ and $\overline{k}_e = \left[\,0\ -k_{ye}\ k_{\text{in}}\,\right]$, respectively. By applying the boundary conditions, reflection coefficients R_p, R_s and transmission coefficients T_o, T_e can be determined. Our analytical expressions provided in Additional file 1: Section S2 show that these coefficients depend on both the magnitude and direction of the particle velocity.

4.2 Energy loss spectrum of the swift charged particle

The total power dissipation (i.e. the energy loss per particle per second) is evaluated as

$$P = -4\pi \int \mathrm{d}\omega \cdot \int\int\int \mathrm{d}V \mathrm{Re}\left[E(\overline{r},\omega)\cdot \overline{J}(\overline{r},\omega)\right].$$

Detailed derivations provided in Additional file 1: Section S3 show that the total energy loss P takes the following analytical form,

$$P = \frac{q_0^2 v \mu_0}{4\pi}\int_0^{\infty}\mathrm{d}\omega\left[\omega\left(1-\frac{c^2}{\varepsilon_a v^2}\right)u\left(1-\frac{c^2}{\varepsilon_a v^2}\right)\right] + 2q_0 v\int_0^{\infty}\mathrm{d}\omega\int_{-\infty}^{+\infty}\mathrm{d}k_x \mathrm{Re}\left[\frac{k_x R_s + k_{ya}k_z R_p}{\sqrt{k_x^2+k_z^2}}e^{\mathrm{i}k_{ya}y_0}\right],$$

where $u(t)$ is the Heaviside step function. Notably, our method does not consider the secondary particle production, resulting from the interaction between the moving charged particle and high-density dielectrics. However, the consideration of secondary particle production is no longer necessary if we adopt, for example, the multilayered structure as shown in Additional file 1: Fig. S11a in practical applications (see more discussions in Additional file 1: Section S8).

Supplementary Information

The online version contains supplementary material available at https://doi.org/10.1186/s43593-021-00009-5.

Additional file 1: Section S1. Eigenequation of Dyakonov surface waves. Section S2. Calculating fields of surface Dyakonov-Cherenkov radiation. Section S3. Calculating energy loss in surface Dyakonov-Cherenkov radiation. Section S4. Influence of the birefringence on the surface Dyakonov-Cherenkov radiation. Section S5. Dispersion, isofrequency contour of surface dyakonon and electromagnetic properties of surface Dyakonov-Cherenkov radiation. Section S6. Radiation field pattern of surface Dyakonov-Cherenkov radiation. Section S7. Intensity of surface Dyakonov-Cherenkov radiation. Section S8. Practical implementation of surface Dyakonov-Cherenkov detectors.

Acknowledgements
Not applicable.

Authors' contributions
All authors contributed extensively to the work presented in this paper. YL and HH conceived the idea of the research. HH performed the calculation. YL, XL,

LJW and BZ contributed insight and discussion on the results. HH, XL, QY, DL and YL wrote the paper. YL and BZ supervised the project. All authors read and approved the final manuscript.

Funding
Y.L. was sponsored in part by Singapore Ministry of Education (No. MOE2018-T2-2-189 (S), MOE2017-T1-001-239 (RG91/17 (S)), A*Star AME Programmatic Funds (No. A18A7b0058) and National Research Foundation Singapore Competitive Research Program (No. NRF-CRP18-2017-02). B.Z. was sponsored in part by Singapore Ministry of Education (No. MOE2018-T2-1-022 (S), MOE2016-T3-1-006 and Tier 1 RG174/16 (S)). L.J.W. was sponsored in part by the Advanced Manufacturing and Engineering Young Individual Research Grant (No. A1984c0043) from the Science and Engineering Research Council of the Agency for Science, Technology and Research, Singapore. X. L. was sponsored in part by the National Natural Science Foundation of China (NSFC) (No. 62175212), the Fundamental Research Funds for the Central Universities (No. 2021FZZX001-19), and Zhejiang University Global Partnership Fund.

Availability of data and materials
All data generated or analysed during this study are included in this published article and its Additional file.

Declarations

Ethics approval and consent to participate
Not applicable.

Consent for publication
Not applicable.

Competing interests
The authors declare that they have no competing interests.

Author details
[1]School of Electrical and Electronic Engineering, Nanyang Technological University, 50 Nanyang Avenue, Singapore 639798, Singapore. [2]Interdisciplinary Center for Quantum Information, State Key Laboratory of Modern Optical Instrumentation, ZJU-Hangzhou Global Science and Technology Innovation Center, College of Information Science and Electronic Engineering, Zhejiang University, Hangzhou 310027, China. [3]International Joint Innovation Center, ZJU-UIUC Institute, Zhejiang University, Haining 314400, China. [4]Division of Physics and Applied Physics, School of Physical and Mathematical Sciences, Nanyang Technological University, 21 Nanyang Link, Singapore 637371, Singapore. [5]Centre for Disruptive Photonic Technologies, Nanyang Technological University, 21 Nanyang Link, Singapore 637371, Singapore. [6]UMI 3288 CINTRA, CNRS/NTU/THALES, Nanyang Technological University, 50 Nanyang Drive, Singapore 637553, Singapore.

Received: 6 August 2021 Revised: 5 November 2021 Accepted: 20 November 2021
Published online: 04 January 2022

References

1. P.A. Čerenkov, Visible light from pure liquids under the impact of γ-rays. Dokl. Acad. Sci. URSS **2**, 451–457 (1934)
2. P.A. Čerenkov, Visible radiation produced by electrons moving in a medium with velocities exceeding that of light. Phys. Rev. **52**, 378 (1937)
3. I.E. Tamm, I.M. Frank, Coherent radiation of fast electrons in a medium. Dokl. Acad. Sci. URSS **14**, 107–112 (1937)
4. O. Chamberlain, E. Segrè, C. Wiegand, T. Ypsilantis, Observation of antiprotons. Phys. Rev. **100**, 947 (1955)
5. J.J. Aubert et al., Experimental observation of a heavy particle. J. Phys. Rev. Lett. **33**, 1404 (1974)
6. V. Ginis, J. Danckaert, I. Veretennicoff, P. Tassin, Controlling Cherenkov radiation with transformation-optical metamaterials. Phys. Rev. Lett. **113**, 167402 (2014)
7. C. Roques-Carmes, N. Rivera, J.D. Joannopoulos, M. Soljačić, I. Kaminer, Nonperturbative quantum electrodynamics in the Cherenkov effect. Phys. Rev. X **8**, 041013 (2018)
8. X. Lin et al., Controlling Cherenkov angles with resonance transition radiation. Nat. Phys. **14**, 816 (2018)
9. T. Ypsilantis, J. Séguinot, Theory of ring imaging Cherenkov counters. Nucl. Instrum. Methods A **343**, 30–51 (1994)
10. G. Adamo et al., Light well: a tunable free-electron light source on a chip. Phys. Rev. Lett. **103**, 113901 (2009)
11. F. Liu et al., Integrated Cherenkov radiation emitter eliminating the electron velocity threshold. Nat. Photonics **11**, 289 (2017)
12. N.V. Sapra et al., On-chip integrated laser-driven particle accelerator. Science **367**, 79–83 (2020)
13. K. Wang et al., Coherent interaction between free electrons and a photonic cavity. Nat. Commun. **582**, 50–54 (2020)
14. M. Shentcis et al., Tunable free-electron X-ray radiation from van der Waals materials. Nat. Photonics **14**, 1–7 (2020)
15. X. Lin et al., A Brewster route to Cherenkov detectors. Nat. Commun. **12**, 1–7 (2021)
16. D.K. Gramotnev, S.I. Bozhevolnyi, Plasmonics beyond the diffraction limit. Nat. Photonics **4**, 83 (2010)
17. O. Takayama et al., Dyakonov surface waves: a review. Electromagnetics **28**, 126–145 (2008)
18. Y. Yang et al., A general theoretical and experimental framework for nanoscale electromagnetism. Nature **576**, 248–252 (2019)
19. H. Hu, X. Lin, Y. Luo, Free electron radiation engineering via structured enviroments. Prog. Electromagn. Res. **171**, 75–88 (2021)
20. J. Pendry, L. Martin-Moreno, F. Garcia-Vidal, Mimicking surface plasmons with structured surfaces. Science **305**, 847–848 (2004)
21. A. Grigorenko, M. Polini, K. Novoselov, Graphene plasmonics. Nat. Photonics **6**, 749 (2012)
22. W.L. Barnes, A. Dereux, T.W. Ebbesen, Surface plasmon subwavelength optics. Nat. Commun. **424**, 824–830 (2003)
23. H. Hu, J. Zhang, S.A. Maier, Y. Luo, Enhancing third-harmonic generation with spatial nonlocality. ACS Photonics **5**, 592–598 (2017)
24. Z. Liu, H. Lee, Y. Xiong, C. Sun, X. Zhang, Far-field optical hyperlens magnifying sub-diffraction-limited objects. Science **315**, 1686–1686 (2007)
25. K.V. Sreekanth et al., Extreme sensitivity biosensing platform based on hyperbolic metamaterials. Nat. Mater. **15**, 621 (2016)
26. D. Lu, J.J. Kan, E.E. Fullerton, Z. Liu, Enhancing spontaneous emission rates of molecules using nanopatterned multilayer hyperbolic metamaterials. Nat. Nanotechnol. **9**, 48 (2014)
27. Z. Jacob, Hyperbolic phonon–polaritons. Nat. Mater. **13**, 1081–1083 (2014)
28. G. Hu et al., Topological polaritons and photonic magic angles in twisted α-MoO 3 bilayers. Nature **582**, 209–213 (2020)
29. C. Maciel-Escudero, A. Konečná, R. Hillenbrand, J. Aizpurua, Probing and steering bulk and surface phonon polaritons in uniaxial materials using fast electrons: hexagonal boron nitride. Phys. Rev. B **102**, 115431 (2020)
30. S. Liu et al., Surface polariton Cherenkov light radiation source. Phys. Rev. Lett. **109**, 153902 (2012)
31. S. Xi et al., Experimental verification of reversed Cherenkov radiation in left-handed metamaterial. Phys. Rev. Lett. **103**, 194801 (2009)
32. H. Chen, M. Chen, Flipping photons backward: reversed Cherenkov radiation. Mater. Today **14**, 34–41 (2011)
33. L.J. Wong, I. Kaminer, O. Ilic, J.D. Joannopoulos, M. Soljačić, Towards graphene plasmon-based free-electron infrared to X-ray sources. Nat. Photonics **10**, 46–52 (2016)
34. P. Genevet et al., Controlled steering of Cherenkov surface plasmon wakes with a one-dimensional metamaterial. Nat. Nanotechnol. **10**, 804–809 (2015)
35. Z. Duan et al., Observation of the reversed Cherenkov radiation. Nat. Commun. **8**, 14901 (2017)
36. Y. Yang et al., Maximal spontaneous photon emission and energy loss from free electrons. Nat. Phys. **14**, 894–899 (2018)
37. H. Hu et al., Nonlocality induced Cherenkov threshold. Laser Photonics Rev. **14**, 2000149 (2020)
38. H. Hu et al., Directing Cherenkov photons with spatial nonlocality. Nanophotonics **9**, 3435–3442 (2020)

39. S.A. Maier, *Plasmonics: Fundamentals and Applications* (Springer Science & Business Media, New York, 2007)
40. M.I. Dyakonov, New type of electromagnetic wave propagating at an interface. J. Exp. Theor. Phys. **67**, 714–716 (1988)
41. O. Takayama, L. Crasovan, D. Artigas, L. Torner, Observation of Dyakonov surface waves. Phys. Rev. Lett. **102**, 043903 (2009)
42. J. Gomis-Bresco, D. Artigas, L. Torner, Anisotropy-induced photonic bound states in the continuum. Nat. Photonics **11**, 232 (2017)
43. O. Takayama, D. Artigas, L. Torner, Lossless directional guiding of light in dielectric nanosheets using Dyakonov surface waves. Nat. Nanotechnol. **9**, 419 (2014)
44. D. Artigas, L. Torner, Dyakonov surface waves in photonic metamaterials. Phys. Rev. Lett. **94**, 013901 (2005)
45. R.K. Bock, A. Vasilescu, in *The Particle Detector BriefBook*. (Springer, Berlin, 1998)
46. J. Tao, Q.J. Wang, J. Zhang, Y. Luo, Reverse surface-polariton Cherenkov radiation. Sci. Rep. **6**, 30704 (2016)
47. I.H. Malitson, M.J. Dodge, Refractive-index and birefringence of synthetic sapphire. J. Opt. Soc. Am. **62**, 1405–1405 (1972)
48. P.B. Johnson, R.-W. Christy, Optical constants of the noble metals. Phys. Rev. B **6**, 4370 (1972)
49. T. Qu et al., Cherenkov radiation generated in hexagonal boron nitride using extremely low-energy electrons. Nanophotonics **9**, 1491–1499 (2020)
50. M.B. Bouchard et al., Swept confocally-aligned planar excitation (SCAPE) microscopy for high-speed volumetric imaging of behaving organisms. Nat. Photonics **9**, 113–119 (2015)